3D Printed Lithium Metal Full-Battery Based on High-Performance Three-dimensional Anode Current Collector

Chenglong Chen[a], Shaopeng Li[b], Peter H.L. Notten[c], Yuehua Zhang[d], Qingli Hao[a]*, Xiaogang Zhang[b]*, Wu Lei[a]*,

a School of Chemical Engineering, Nanjing University of Science and Technology, Nanjing, 210094, China. 200 Xiaolingwei street, Xuanwu District, Nanjing City, Jiangsu Province

b Jiangsu Key Laboratory of Electrochemical Energy Storage Technology, College of Material Science and Engineering, Nanjing University of Aeronautics and Astronautics, Nanjing, 210016, China. shaopengli@nuaa.edu.cn

c Eindhoven University of Technology, P.O. Box 513, 5600 MB Eindhoven, The Netherlands.

Forschungszentrum Jülich (IEK-9), D-52425, Jülich, Germany.

d School of Chemistry and Chemical Engineering, Nantong University, Nantong, 226007, China.

Corresponding Authors: Tel.: +86-25-84315943; Fax: +86-25-84315190

E-mail: leiwuhao@njust.edu.cn (W. Lei); qinglihao@njust.edu.cn (Q.L. Hao).

azhangxg@nuaa.edu.cn (X.G. Zhang)

Abstract

A three-dimensional (3D) printing method has been developed for the lithium anode base on 3D-structured copper mesh current collectors. Through in-situ observations and computer simulations, the deposition behavior and mechanism of lithium ions in the 3D copper mesh current collector are clarified. Benefiting from the characteristics that the large pores can transport electrolyte and provide space for dendrites growth, and the small holes guide the deposition of dendrites, 3D Cu mesh anode has an excellent deposition and stripping capability (50 mAh cm^{-2}), high-rate capability (50 mA cm^{-2}), and long-term stable cycle (1000 h). A full lithium battery with $LiFePO_4$ cathodes based on this anode delivers a good cycle life. Moreover, a 3D fully printed lithium sulfur battery with the 3D printed high-load sulfur cathode can easily charge mobile phones and light up 51 LED indicators, which provides a great potential for the practicability of lithium-metal batteries with the characteristic of high energy densities. Most importantly, this unique and simple strategy is also feasible to solve the dendrite problem of other secondary metal batteries. Furthermore, this method has great potential in the continuous mass production of electrodes.

Keywords: 3D printing, lithium metal anode, lithium dendrites, high-rate, deposition behavior

1. Introduction

Since the emergence of various intelligent equipment and electric vehicles, Rechargeable Energy Storage System represented by lithium-ion battery has been extensively applied[1, 2]. However, after nearly 30 years of commercial applications and development of lithium-ion battery system, the theoretical limit of the energy density has been approached, which is difficult to meet the higher demands for energy density, power density, safety and cycle life of secondary batteries in emerging industries[3-5]. Lithium anode not only has a very high theoretical specific capacity (3860 mAh g^{-1}), but also has the lowest reduction potential in lithium metal batteries (LMB)[6]. Moreover, lithium is the lowest density alkali metal (0.54 g cm^{-3})[7]. The above factors indicate that lithium metal has an outstanding energy density per unit mass, which is the best energy storage material for secondary batteries in the future. Lithium metal batteries, such as Li−S, Li−Se, and Li−O_2 batteries, based on lithium metal anode, have become the most attractive new generation of high specific energy secondary battery energy storage systems [8-10].

However, lithium metal, as the anode for batteries, still faces many problems and challenges[11]. Among them, the safety issue is the biggest obstacle restricting its commercial application[12, 13]. Because many sharp dendrites induce large stresses on the separator, which might cause the separator puncture and thermal runaway problems, including battery short circuit, gas production, fire, and even explosion. At the same time, during the lithium metal deposition/peeling cycle, the solid electrolyte interphase (SEI) ruptures because lithium metal volume continuously shrinks and expands. The

exposed fresh lithium surface will continue to react with the electrolyte to produce new SEI[14-17]. Eventually, the electrolyte becomes depleted and the lithium metal electrode is severely corroded, which leads to battery failure. Therefore, researches have been carried out for the solution to the above failures[11]. Among them, three-dimensional (3D) frameworks have been proved to effectively inhibit dendrite growth and enhance the cycle efficiency of lithium metal anodes[18-22]. The 3D framework of lithium metal anodes can provide a higher specific surface area, faster electron transfer, more ion adsorption and electrochemical reaction sites, and reduce the polarization voltage of the lithium metal deposition and stripping process. Therefore, researchers developed a series of 3D-structured lithium metal anodes based on graphene[23], artificial graphite[24], carbon fibers[25, 26], porous copper[27-30], nickel foam[31-34], etc. 3D printing technology is very friendly, simple and fast for the preparation of similar three-dimensional structures.

The advancement of 3D printing technologies provides new possibilities for solving the outstanding challenge of lithium metal battery safety. 3D printing is an environmentally friendly technology with cost-effectiveness since it owns a strategy of additive manufacturing by depositing materials as needed[35-40], which minimizes the waste of materials, and it is more energy-efficient and environmentally friendly than traditional methods. Moreover, 3D printing has excellent size and shape controllability[41, 42]. Using suitable ink materials, various complex patterns can be manufactured quickly, precisely and flexibly. The design and controlled mass production of new electrode materials and their devices are achievable through 3D

printing technology[43, 44].

In the paper, a method of 3D printing was developed for preparing 3D metal current collectors for high-performance lithium metal battery that has greatly improved safety and cycling stability. 3D Cu meshes were fabricated by 3D printing technology based on direct ink writing. Copper powder pastes with appropriate viscosity were extruded through a 3D printer to form a grid structure. Continuous mass production can be realized via 3D printing technology. The 3D copper mesh has a high aspect ratio structure in a small volume, which provides more electroactive sites and holds the deposited Li metal inside, while making the electric field distribution more uniform to effectively control the current density. As far as we know, the method we developed for the 3D printing of metal current collectors in this work has never been reported. We believe that this method is universal. For example, using other metal powder instead of Cu powder will lead to a similar conclusion.

Combined with computer simulations, experimental investigations were carried out to confirm that the 3D printed skeleton can induce dendrite growth inside the electrode at low current density. The growth direction of most dendrites is changed from vertical to parallel to the separator, thereby solving the safety problem of dendrite piercing the separator at high current densities. Meanwhile, the open structure of the 3D Cu mesh can effectively reduce the occurrence of dead lithium and improve the coulombic efficiency and battery cycle life. It can also alleviate the huge volume change in the process of the charging and discharging of the lithium metal anode by providing structural support and improve the battery structural stability. The results demonstrate

that the 3D Cu mesh has a significant superiority in improving the rate performance and cycle life of lithium metal anodes. In order to improve the safety of the battery under ultra-high current density, a strategy of pre-depositing lithium on the Cu mesh was adopted. The safe charging and discharging of the ultra-high current density of 50 mA cm^{-2} surpasses most of the reported studies[27, 28, 45, 46]. Furthermore, lithium batteries with high performance were successfully assembled with $LiFePO_4$ as cathode and lithium deposited on 3D Cu mesh as anode. And a representative 3D fully printed lithium-sulfur battery is assembled with a 3D printed high-load sulfur cathode and can easily light up 51 LED indicators. This work indicates that the 3D printed Cu mesh has broad application potential in practical lithium metal batteries with high energy density and high safety.

2 Results and Discussions

2.1 Fabrication and characterization of 3D Cu current collectors

Figure 1 shows the printing process of 3D Cu mesh. There are roughly three steps in the mass production process. The first step is to prepare the printing paste. Copper powder, PVDF and NMP were mixed in proportion using a planetary vacuum mixer for ten minutes (**Figure 1a**). PVDF was added as a binder between the Cu particles. NMP was used as solvent to adjust the viscosity of the paste. In order to keep the shape of extruded lines from collapsing, high-viscosity pastes were synthesized by adding a small amount of NMP. In the second step, the Cu paste was printed into a grid structure through a home-made 3D printer. The piston was pushed by air pressure to extrude the paste from the needle. The syringe was equipped with a ring electric heater and a temperature controller to improve the fluidity of the high viscosity paste for extrusion through a 200 μm needle. At the same time, when the paste was extruded onto the slide, the electric heating platform quickly evaporated the NMP in the paste to induce solidification (**Figure 1b**). The final step is to remove the PVDF from the printed Cu mesh. Because PVDF is a poorly conducting polymer, the conductivity of copper mesh will be greatly reduced when copper particles are bonded by PVDF. PVDF was therefore removed by the heat treatment method. The 3D printed Cu mesh was calcined in air to remove PVDF. Simultaneously, copper was also oxidized. Therefore, the copper oxide was calcined in a hydrogen atmosphere, and the 3D Cu mesh configuration was finally obtained (**Figure 1b**). The powerful mass production capabilities of 3D printer technology are shown in **Figure 1c**. The 3D Cu structures

were programmed and continuously printed (Supporting Video 1).

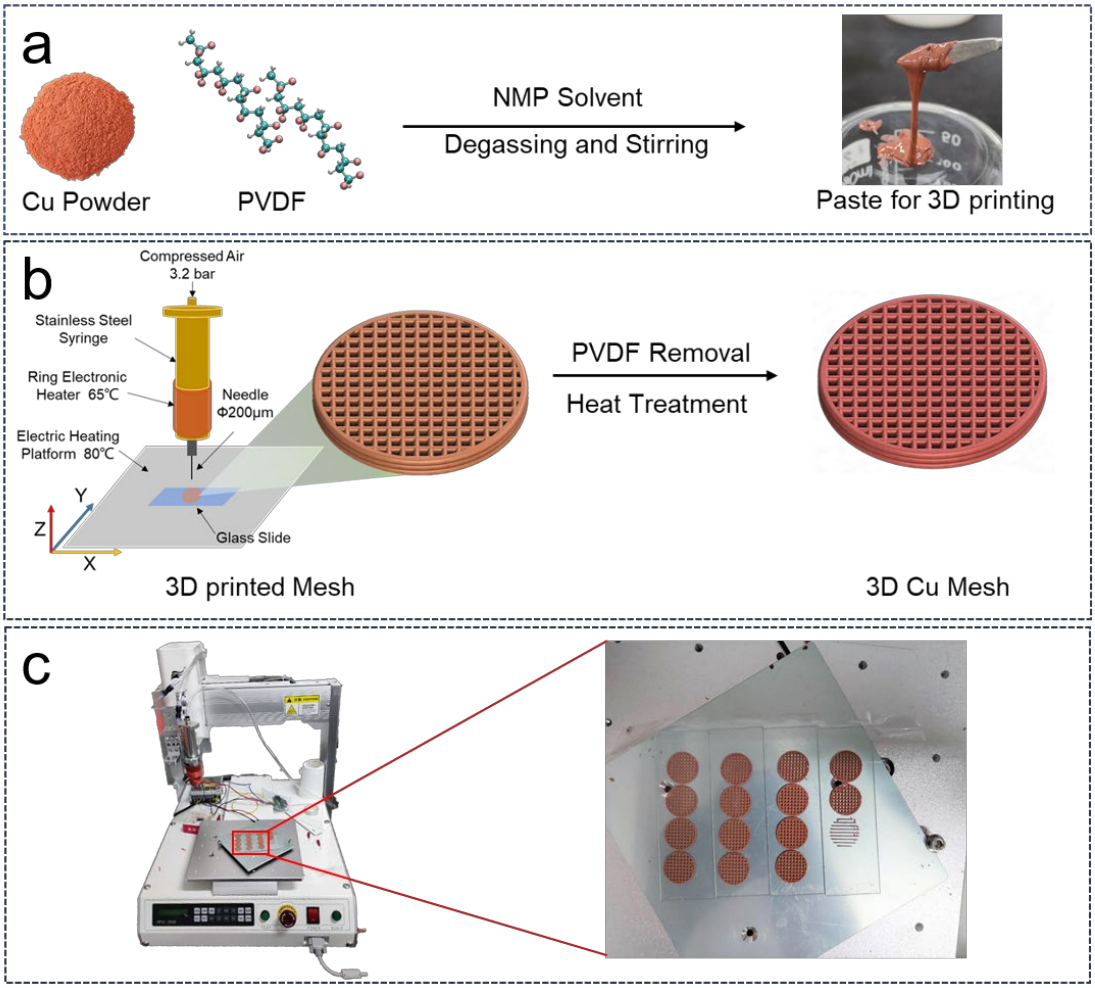

Figure 1. Preparation process of 3D printed Cu mesh. (a) Synthesis of paste. (b) Schematic diagram of 3D printing mechanism and post-processing process of Cu mesh. (c) Mass-produced 3D printed Cu meshes.

Scanning electron microscope (SEM) was adopted to observe structural changes of 3D printed samples during the preparation process. The morphology of 3D Cu mesh before and after heat treatment is shown in **Figure 2a-c** and **Figure 2d-f**, respectively. The internal morphology of the 3D Cu mesh is shown in **Figure 2g-i**. As exhibited in **Figure 2a–c**, shape of 3D Cu mesh after printing is well maintained due to the rapid solidification of PVDF, and the individual layers are nicely merged. Due to layer-by-

layer printing and layer-by-layer solidification process, there are clear boundaries between the individually printed layers (**Figure 2c**). These interfaces rely on the binder to maintain its three-dimensional structure, but the 3D Cu mesh has lost its electrical conductivity.

Figure 2d-f demonstrate the morphology of the 3D copper mesh after heat treatment. Obviously, the vertical and horizontal filaments are fused together like a weld, creating a large number of bridges to facilitate electronic transport in all directions. It can be seen in **Figure 2d** and **e** that the filament width in this example is about 220 μm. And the distance of about 400 μm between two adjacent filaments can also be found, forming a uniform array of square holes. The cross-section of **Figure 2f** shows that a single printed layer of 3D Cu mesh has the thickness of 200 μm, and the total printed thickness of the three layers is 600 μm. These large deep holes not only serve as transport channels for the electrolyte, but also provide enough space for the growth and expansion of dendrites. When the paste was cured no obvious holes were found at the surface of the printed filament (**Figure 2g**). However, after the polymer binder was treated at 620°C, many small holes appeared (**Figure 2h**). Most of the small pores come from the space occupied by PVDF and the space where particles accumulate during solidification. As shown in the magnified SEM image of **Figure 2 i**, after the printed Cu mesh was sintered and reduced at 580°C, a well-designed 3D mesh with hierachical porous structure was preserved, and the Cu particles formed an integrally connected skeleton through sintering, thereby ensuring the excellent mechanical strength and conductivity of 3D Cu skeleton. Finally, the hierachical porous 3D Cu mesh is used as

current collector where the large opening can store the electrolyte and provide more space for dendrite growth, and small pores may guide dendrite deposition.

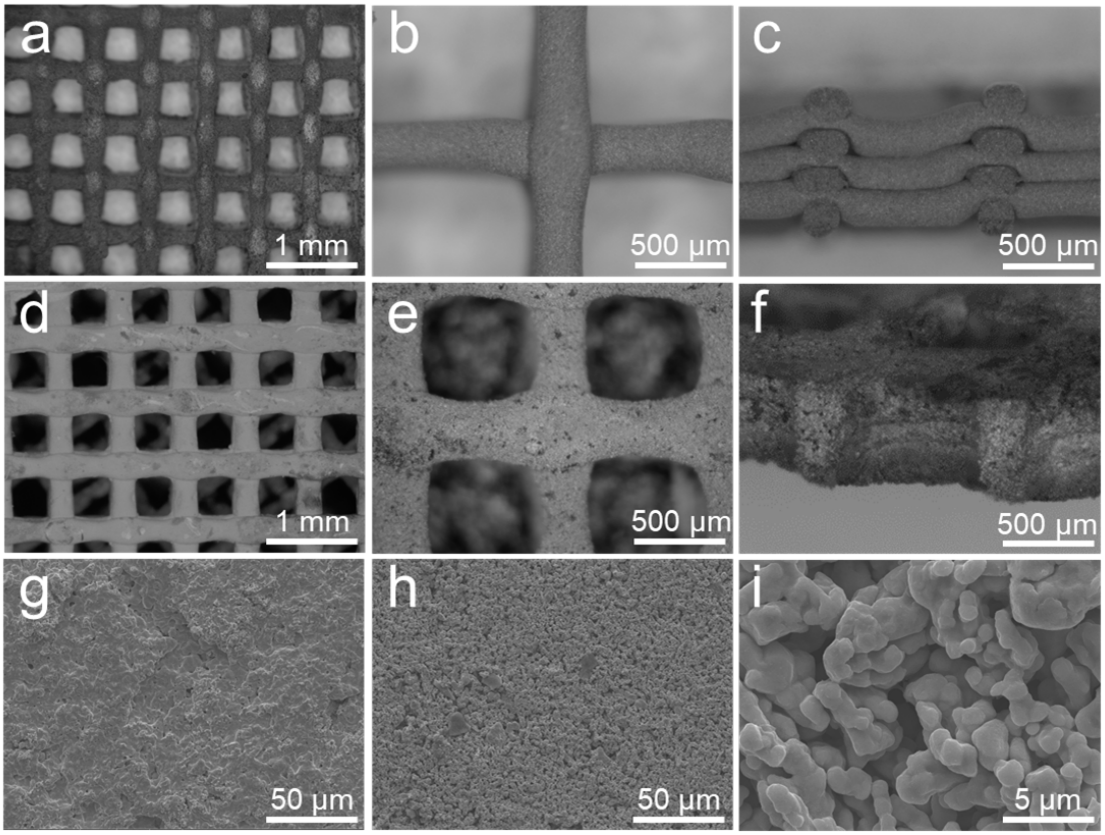

Figure 2. The morphology of 3D Cu mesh before (a-c) and after (d-f) heat treatment. (g-i) The internal morphology of 3D Cu mesh.

2.2 Simulations and in-situ observation of lithium deposition in 3D-structures current collectors

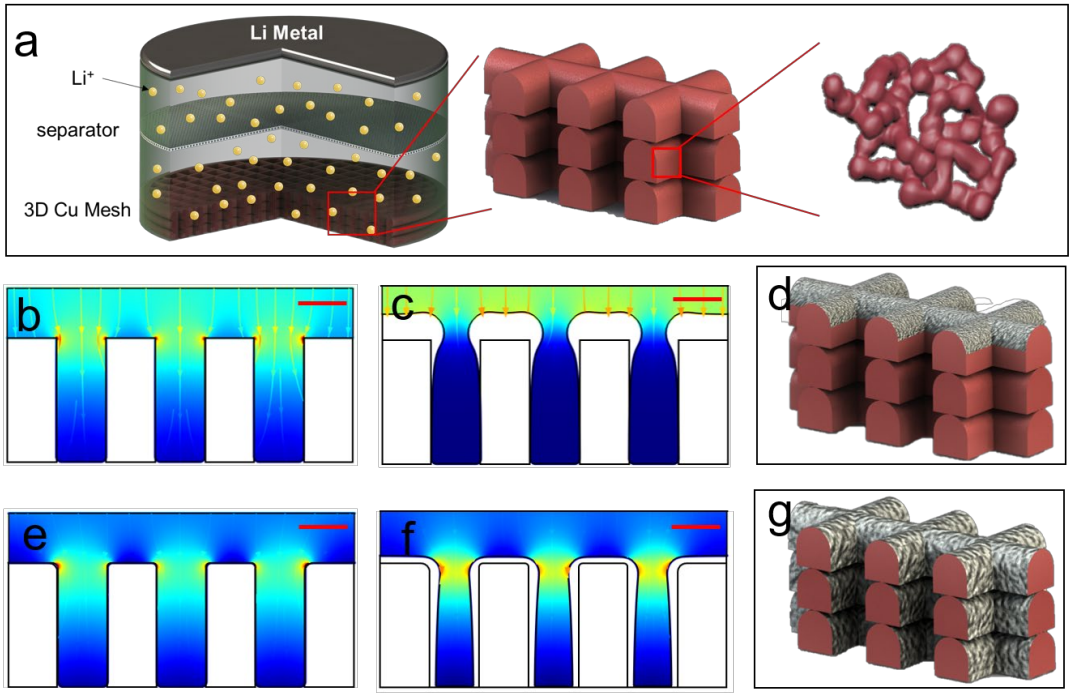

Figure 3. (a) Schematic diagram of the inside of the coin cell. Simulation diagram of dendrite distribution at high (b-d) and low (e-g) current densities. The red scale bar in the simulation diagram is 250 μm.

For better understanding of the deposition behavior of 3D copper meshes, the distribution of current density in the process of deposition and the evolution of the lithium morphology under different current densities were investigated through COMSOL simulations and optical microscope[16, 45, 47]. **Figure 3a** schematically shows the cross-sectional structure of a coin-type battery used for testing. Lithium metal and 3D copper mesh are the anode and cathode, respectively, and common 1,3-dioxolane （DOL）/dimethoxy ethane（DME）based electrolyte is used in the coin-type batteries. The simplification of the 3D copper mesh model is to reduce plenty of calculations during simulation. As it is shown in **Figure 3b** and **3e**, simulation results indicate the two-dimensional distribution of current density of 3D copper mesh from the aspect of

cross-section. 25 mA cm^{-2} and 0.5 mA cm^{-2} were set for the current density. In current density distribution chart, the colors from blue to red define the relative current density from low to high. Obviously, the corner of the electrode surface protrusion shows the highest current density. These results are in accordance with the theory of lightning rod, showing the charge density on the surface of conductor increases with the curvature of the conductor[48]. Subsequently, as shown in **Figure 3c** and **3f**, the evolution of the morphology of lithium during the deposition was simulated by combining the deformation geometry function in COMSOL, with the two current densities mentioned above[49]. The lithium is preferentially deposited at 25 mA cm^{-2}, a high current density, on the top of 3D copper mesh like a mushroom head (**Figure 3c**). **Figure 3d** schematically shows the deposition result. On the contrary, the deposition position of lithium is located on the sidewall of the channel and the top of 3D copper mesh at 0.5 mA cm^{-2}, a low current density. **Figure 3f** and **3g** show that the layer thickness is uniform.

In order to further confirm the simulation results, a digital optical microscope was used to monitor the lithium deposition process in-situ at different current densities. The growth process of lithium dendrites is observed in-situ through an assembled sealed two-electrode transparent battery system (**Figure 4a**). A lithium sheet is used as working electrode, and the 3D copper mesh is aligned parallel to it. Thin wires are used to connect them to the electrochemical workstation.

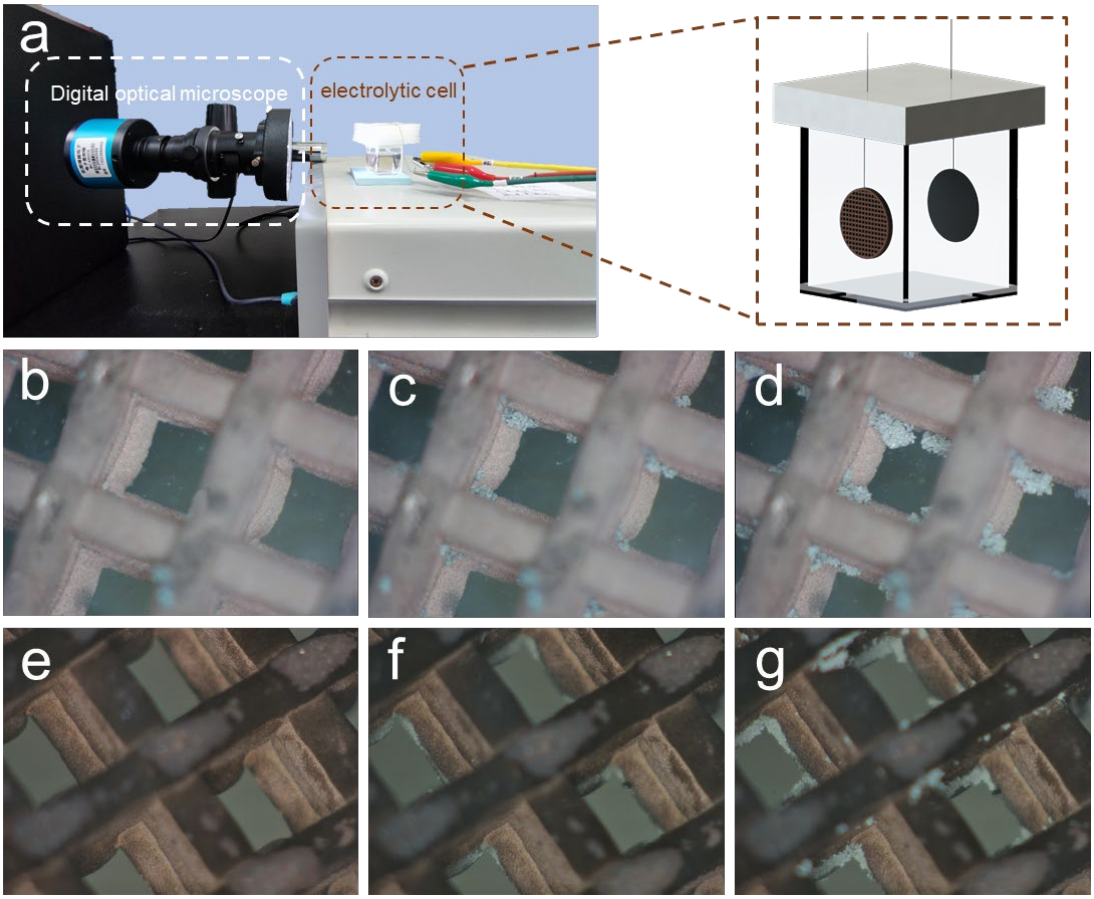

Figure 4. (a) Schematic diagram of the equipment of a digital optical microscope for in-situ observations. Morphology changes of lithium deposition at the current density of 0.5 mA cm^{-2} (b-d) and 25 mA cm^{-2} (e-g).

Morphological changes of lithium deposition at 0.5 mA cm^{-2} (b-d**)** and 25 mA cm^{-2} (e-g), as the current density are shown in **Figure 4**. Benefiting from the open structure of 3D copper mesh, morphological changes with deposition time can be clearly observed. Lithium dendrites slowly nucleate on the sidewall of the channel and grow at 0.5 mA cm^{-2} (Supporting Video 2). By comparison, there is almost no lithium deposited on the sidewall of the channel at 25 mA cm^{-2} which is a high current density, and lithium dendrites only grow on the top of 3D copper mesh (**Supporting Video 3**). All results

verify the fact that the current density is determining the lithium deposition morphology, and the distribution of lithium dendrites becomes more concentrated at higher current densities, and more dispersed at lower current densities.

2.3 Electrochemical performance of 3D anodes

To investigate an equal amount of Li (5 mAh) has been deposited at 0.5 mA cm^{-2} and 10 mA cm^{-2} for the investigation of Li's deposition behaviors on 3D Cu mesh.

Figure 5a-c shows that at 0.5 mA cm^{-2}, a small amount of Li unavoidably deposited on the top surface of 3D Cu mesh, but it did not cover the surface. From **Figure 5b** and **c**, it is obvious that most of the Li has been deposited on the inner Cu skeleton and are uniformly wrapped on the Cu particles. The cross-sectional SEM images (**Figure 5h** and **i**) reveal that most of the deposited Li nuclei and dendrites are stored in the small holes of the 3D Cu mesh structure. This is similar to the shape found in former reports[50, 51]. The first stage of deposition shows the form of spherical lithium nuclei, however, the lithium nuclei grow rapidly along the longitudinal direction in later growth stage, while it grows very slowly in the other direction (width). The large pores of the 3D Cu mesh can store a large amount of electrolyte, which infiltrate the porous skeleton of Cu filaments to form a 3D channel network for Li ion diffusion. It benefits to help and promote the mass transfer of ions. Moreover, the large surface area of porous Cu skeleton helps for the reduction of electric field. Consequently, the lithium nuclei's growth in all directions can be promoted through the uniformity of Li^+ concentration and electric field distribution and the lithium nuclei finally becomes a mulberry shape structure (**Figure 5c**). The granular lithium grows uniformly at the Cu surface.

Conversely, mass transfer becomes the determining factor for the deposition morphology of lithium at high current densities. The lithium deposition layer is mainly concentrated on the upper surface at a current density of 10 mA cm^{-2} (**Figure 5d** and **g**). From the cross-sectional SEM image, we can see that area covered by the deposited lithium extends from the upper surface of the first layer to its half height of the side surface. This is consistent with the results obtained from previous COMSOL simulations and in-situ optical microscope observations. All results in Figure 5 show that the 3D structure of Cu mesh skeleton can provide a wide range of reaction interfaces during deposition at low current density, and the top layer with a curved surface can extend the deposition position to the side at the high current density. Therefore, regardless of low or high current density, 3D Cu mesh can be used for the realization of the high stability of the lithium anode.

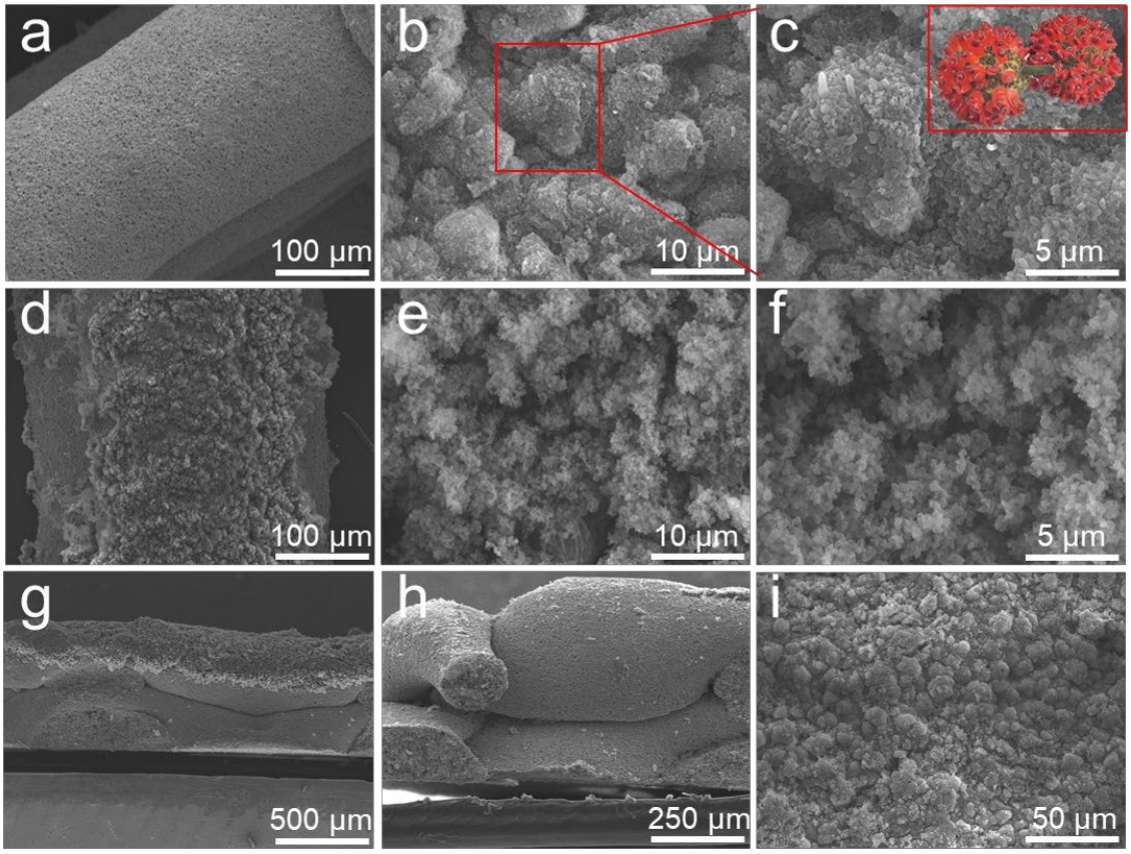

Figure 5. SEM images of the surface morphology of 3D Cu mesh at 0.5 mA cm^{-2} (a-c) and at 10 mA cm^{-2} (d-f). The cross-sectional SEM images of 3D Cu mesh at 10 mA cm^{-2} (g) and 0.5 mA cm^{-2} (h and i). Li deposition capacity is 5 mAh.

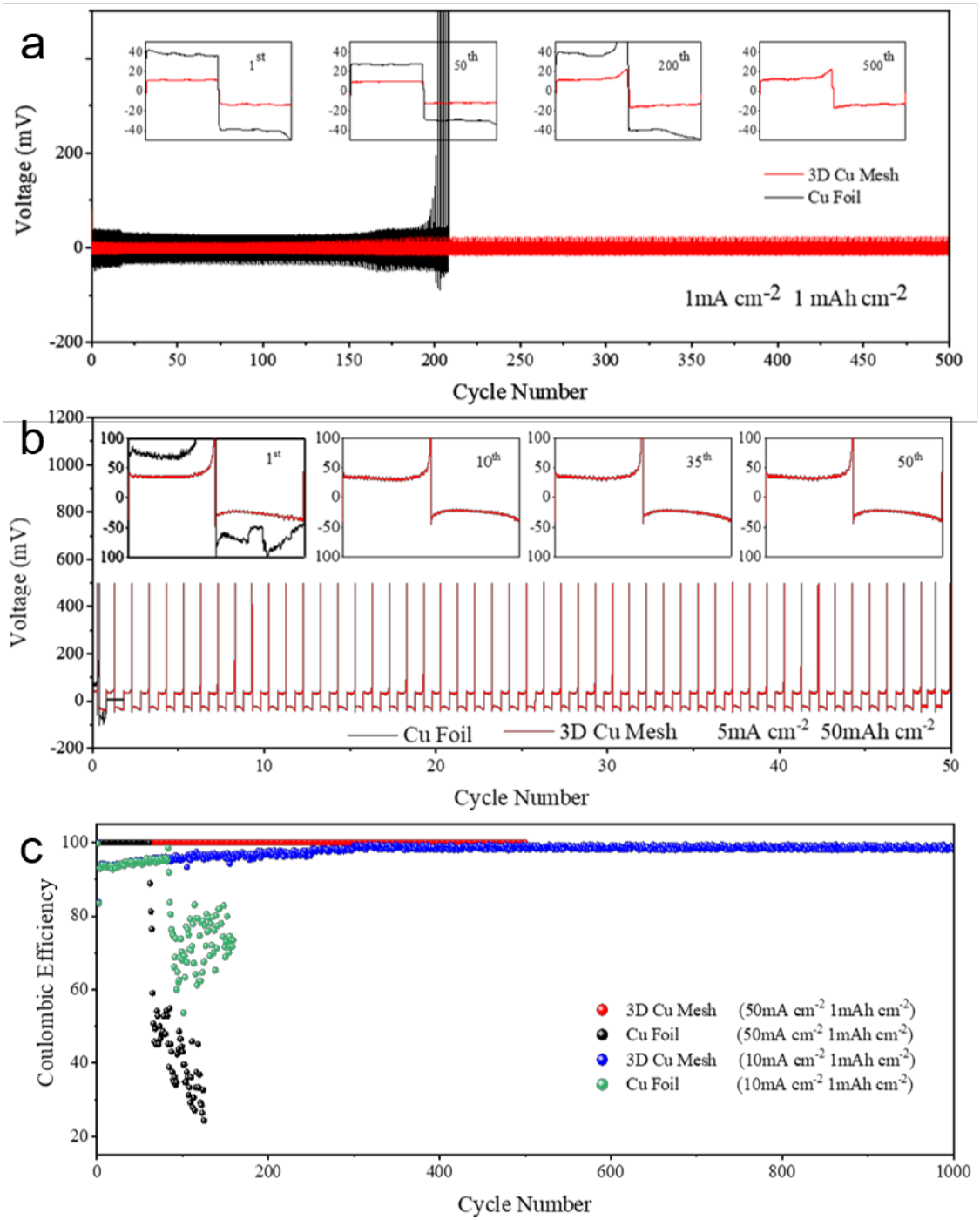

Figure 6. (a) Galvanostatic cycling (1 mA cm^{-2}) of a 3D Cu and planar Cu foil electrode with stripping/plating capacity of 1 mAh cm^{-2}. (b) Cycling of a 3D Cu and planar Cu foil electrode at 5 mA cm^{-2} with a capacity of 50 mAh cm^{-2}. (c) Coulombic efficiency of 3D and planar Cu electrode with a capacity of 1 mAh cm^{-2} and different current density of 50 mA cm^{-2} and 10 mA cm^{-2}.

For the further evaluation of the cycling stability of lithium metal anodes deposited

on different Cu current collectors (3D mesh or planar), we conducted cycling experiments of a half-cell of Li metal battery at various current densities. The galvanostatic plating stripping voltage curves at various cycle numbers are presented as insets in **Figure 6**. For 3D Cu mesh electrode, there exists a stable voltage plateau at 1 mA cm^{-2} in each cycle, 1 mAh cm^{-2}, as the cycle capacity (red curves in the insets of **Figure 6a**). The overpotential is maintained at 20 mV for 500 cycles, which indicates that more active sites are provided for lithium nucleation and deposition by 3D Cu mesh electrode. The overpotential of the planar Cu foil electrode, on the other hand, shows a gradual increase after 150 cycles, and amounts to more than 40 mV after 200 cycles (black voltage curves). This represents the continuously aggravated polarization of the plating and stripping process. It is known to us all that long cycle life can be achieved by plenty of electrolyte[15]. The 3D Cu mesh anode, which stores a large amount of electrolyte, can avoid battery drying up and prevent the polarization of the electrode.

3D Cu anode can still operate stably for 50 cycles when current density and capacity achieves 5 mA cm^{-2} and 50 mAh cm^{-2} respectively (**Figure 6b**). When a copper foil anode is cycled at 50 mAh cm^{-2}, a high capacity, the cell becomes short-circuited already during the first cycle of (dis)charge. This is because the rapid growth of lithium dendrites leads to separator puncturing. This further confirms electrolyte drying at a low current density and short circuit at a high current density mainly led to the failure of lithium metal batteries. The hierarchical porous structure of the 3D Cu mesh takes advantage of its high electrolyte storage capacity and larger dendrite growth space, which provides enough Li^+ supplements and the rapid inner Li^+ transport, and offers

plenty of space for volume changes during cycling.

High-power devices such as electric vehicles and electric airplanes urgently require batteries with higher power density. High-power batteries can be quickly charged and discharged. However, for lithium metal batteries, high power density means deposition and peeling of ultra-high current density. The dendrite growth rate is faster and the morphology is sharper, which leads to more severe safety problems. Here, we realized safe charging and discharging with ultra-high current density through the pre-deposited 3D Cu mesh.

Furthermore, the 3D copper mesh also exhibits an excellent cycle stability during the charge and discharge tests at ultra-high current densities (10 mA cm^{-2} and 50 mA cm^{-2}) (**Figure 6c**). The coulombic efficiency of the 3D Cu mesh anode can reach 99.4% after 1000 cycles at a current density (10 mA cm^{-2}), and maintain more than 98%. This reflects that the three-dimensional architecture of a 3D Cu mesh is beneficial to the formation of a stable SEl film on anode through sufficient electrolyte storage. The low value of the coulombic efficiency in the initial cycle is related to the SEI film formation process. In contrast, the coulomb efficiency of the Cu foil electrode drops rapidly after the 82^{nd} cycle (**Figure 6c**). The high cycling stability and high coulombic efficiency of the 3D copper mesh are much higher than in most reported studies at ultra-high current density[23, 27, 28, 45, 46].

For the ultra-high current density tests, at for instance 50 mA cm^{-2}, we developed a pre-deposition approach to enhance the security performance of lithium battery. Before cycle test at 50 mA cm^{-2}, an ultra-high current density, 3D Cu mesh and Cu foil

were pre-deposited with 12 mAh cm^{-2} of lithium metal at 0.5 mA cm^{-2}, a current density. Thanks to the abundant active sites inside the 3D Cu mesh and the space for dendrite growth, it can stably cycle 500 times at 50 mA cm^{-2}, an ultra-high current density. It has never been previously reported. Coulombic efficiency of copper foil dropped rapidly after the 63rd cycle, which may be caused by short circuits formed by dendrites piercing the separator. Therefore, long cycle life of lithium anodes can be realized through the hierarchical porous structure of the 3D Cu mesh, even at ultra-high current densities.

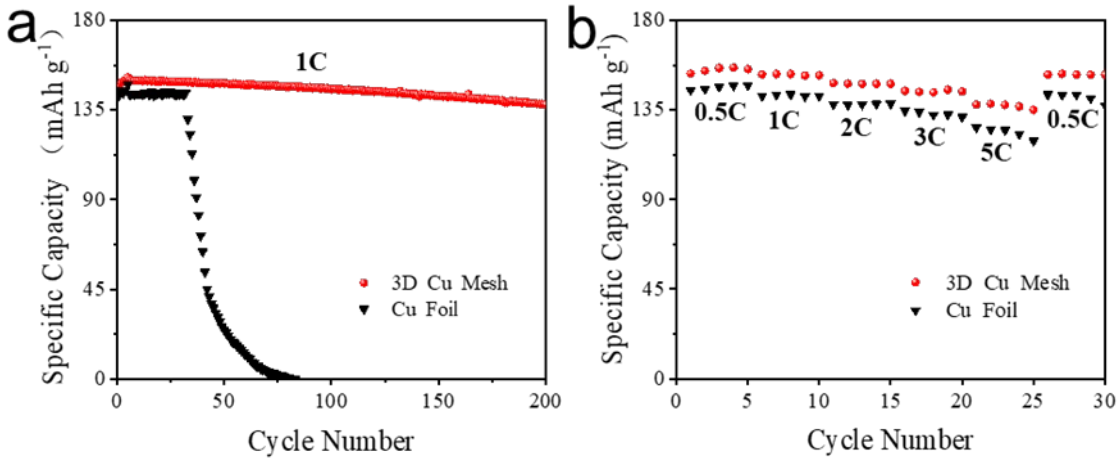

Figure 7. (a) Cycle performance and (b) rate capability of full cells with $LiFePO_4$ as cathode and anode of lithium deposited on either a 3D Cu mesh or planar Cu foil.

Based on the good electrochemical performance of 3D Cu mesh based lithium anodes, full cells were assembled with $LiFePO_4$ as cathodes and lithium deposited on 3D Cu mesh or Cu foil at 0.5 mA cm^{-2} as anodes. The cycle life results and rate capability are shown in **Figure 7**. Although their initial capacity values are not much different from each other, there are significant differences in the cycling stability (**Figure 7a**). 3D Cu Mesh electrode shows a much better cycling stability than that of

the Cu Foil foam electrode. 200 cycles can be easily reached by 3D Cu Mesh electrode with a high capacity retention of 91.8%., whereas failure occurred by a full cell with Cu Foil after only 80 cycles. Moreover, **Figure 7b** shows that $LiFePO_4$ full cell based on 3D Cu mesh exhibits overall advantage in rate performance. Therefore, the 3D copper mesh current collector can effectively ensure the uniform deposition and stripping of lithium and avoid dendrite growth.

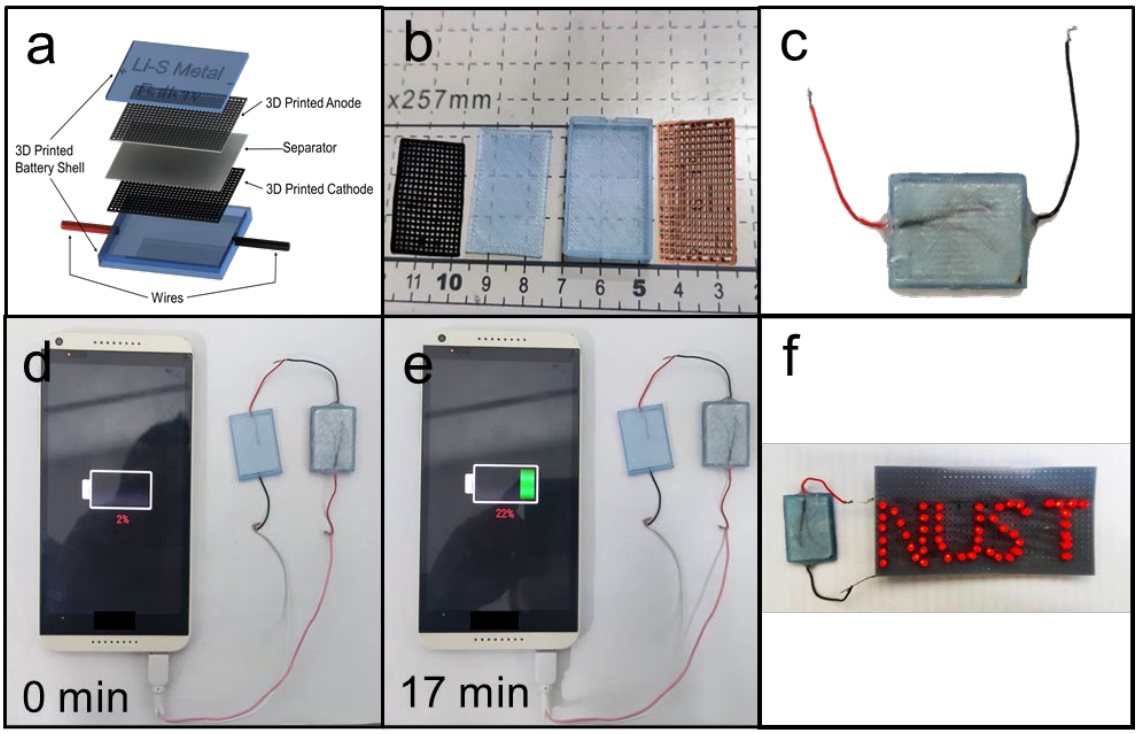

Figure 8. (a) Schematic illustration of a 3D fully printed Li-S battery. (b) The parts used in the actual assembly of the Li-S battery. (c) Assembled 3D fully printed Li-S battery. (d-e) Two lithium-sulfur batteries connected in series can charge the mobile phone from 2% to 22% in 17 minutes. (f) The picture shows that the red LED indicators powered by a 3D fully printed Li-S battery.

Li-S battery is the most representative lithium metal battery. We combined the 3D printed high-load sulfur cathode (9.7 mg cm^{-2}) prepared in the previous work with the 3D printed copper mesh developed in this article to prepare a fully printed Li-S

battery[52]. As shown in **Figure 8(a-c)**, the 3D fully printed Li-S battery contains a battery shell, anode, separator, cathode and wires. Among them, the battery shell is printed by a fused deposition molding 3D printer, and the cathode and anode are printed by a direct writing 3D printer. The 3D copper mesh used as the anode is pre-deposited with 50 mAh lithium metal. Finally, the voltage of the two lithium sulfur batteries in series doubled to meet the charging voltage requirements of the mobile phone, and the battery capacity of the mobile phone increased from 2% to 22% in 17 minutes **Figure 8(d and e)** . And the assembled 3D fully printed Li-S battery easily lights up 51 LED indicators **(Figure 8f)**, which shows that the 3D fully printed battery technology has huge potential in practical applications.

3 Conclusions

In summary, we have developed a 3D Cu mesh prepared with metal powders through 3D printing technology and used it as a collector for Li anodes, which is a universal strategy to inhibit the growth of dendrites of metal batteries and solve their safety problems. This is distinct from the extensively applied strategy of suppressing/delaying dendritic growth. 3D printed structure can efficiently change the distribution of electric field and accommodate electroplated lithium metal. Experiment shows the coulombic efficiency of lithium deposition on the 3D Cu mesh collector remains higher than 98% in 500 cycles and 1,000 cycles of depositing/stripping 1 mAh cm^{-2} lithium at current densities of 1 mA cm^{-2} and 10 mA cm^{-2}, respectively. In addition, the 3D Cu mesh collector achieves a deep stripping and plating capacity of up to 50

mAh cm^{-2} at 5 mA cm^{-2}. The 3D Cu mesh can efficiently prevent the dendrites growth, improve coulomb efficiency and alleviate volume changes. Therefore, this design achieves a long and stable cycle at a low current density, a safe lithium deposition at a high current density, and obtains good cycle efficiency. The anode prepared by this 3D printing technology is expected to have a synergistic effect with other methods of inhibiting dendrites (such as modified electrolyte or electrode materials) for the realization of its practical use in lithium metal battery (Such as all solid-state lithium metal batteries or special-shaped metal batteries).

Since the accuracy of the 3D Cu mesh in the current research work is limited by the 3D printing equipment, we can infer that electroactive area ratio can be further improved if the diameter of the extruded line, the width of the mesh is decreased, and the number density of the mesh cavity is increased. Therefore, more excellent overall performance of lithium anode can be obtained on the basis of higher resolution 3D Cu mesh. In addition, the 3D printing technology with unprecedented consistency and reliability makes the mass production of 3D printing electrode possible in industry. This unique and simple strategy is the first attempt to solve the safety problems caused by dendrites, and will serve as an inspiration to solve similar problems in other secondary metal battery systems.

4 Experimental section

The details are shown in the supporting information.

Acknowledgments

The work was supported by the National Natural Science Foundation of China (Nos. 51572127, 21576138, 51872140, 21875107 and 51802154), Program for NCET-12-0629, Ph.D. Program Foundation of Ministry of Education of China (No.20133219110018), Six Major Talent Summit (XNY-011), Natural Science Foundation of Jiangsu Province (BK20160828), Postdoctoral Science Foundation (1501016B) and PAPD of Jiangsu Province, China. Mr. Chenglong Chen would like to acknowledge the Special Funds for Excellent Doctoral Candidates in NJUST. Thanks eceshi (www.eceshi.cn) for the SEM analysis.

References

[1] Dunn, B.; Kamath, H.; Tarascon, J.-M., Electrical Energy Storage for the Grid: A Battery of Choices. *Science* **2011,** *334* (6058), 928-935.

[2] Chu, S.; Majumdar, A., Opportunities and challenges for a sustainable energy future. *Nature* **2012,** *488* (7411), 294-303.

[3] Liang, Y.; Zhao, C.-Z.; Yuan, H.; Chen, Y.; Zhang, W.; Huang, J.-Q.; Yu, D.; Liu, Y.; Titirici, M.-M.; Chueh, Y.-L.; Yu, H.; Zhang, Q., A review of rechargeable batteries for portable electronic devices. *InfoMat* **2019,** *1* (1), 6-32.

[4] Armand, M.; Tarascon, J. M., Building better batteries. *Nature* **2008,** *451* (7179), 652-657.

[5] Li, Z.; An, Y.; Dong, S.; Chen, C.; Wu, L.; Sun, Y.; Zhang, X., Progress on zinc ion hybrid supercapacitors: Insights and challenges. *Energy Storage Mater.* **2020,** *31*, 252-266.

[6] Zhamu, A.; Chen, G.; Liu, C.; Neff, D.; Fang, Q.; Yu, Z.; Xiong, W.; Wang, Y.; Wang, X.; Jang, B. Z., Reviving rechargeable lithium metal batteries: enabling next-generation high-energy and high-power cells. *Energy Environ. Sci.* **2012,** *5* (2), 5701-5707.

[7] Lin, D.; Liu, Y.; Cui, Y., Reviving the lithium metal anode for high-energy batteries. *Nat. Nanotechnol.* **2017,** *12* (3), 194-206.

[8] Bruce, P. G.; Freunberger, S. A.; Hardwick, L. J.; Tarascon, J.-M., Li–O2 and Li–S batteries with high energy storage. *Nat. Mater.* **2012,** *11* (1), 19-29.

[9] Xia, H.; Xie, Q.; Tian, Y.; Chen, Q.; Wen, M.; Zhang, J.; Wang, Y.; Tang, Y.; Zhang, S., High-efficient CoPt/activated functional carbon catalyst for Li-O2 batteries. *Nano Energy* **2021,** *84*, 105877.

[10] Zhang, D.; Dai, A.; Fan, B.; Li, Y.; Shen, K.; Xiao, T.; Hou, G.; Cao, H.; Tao, X.; Tang, Y., Three-Dimensional Ordered Macro/Mesoporous Cu/Zn as a Lithiophilic Current Collector for Dendrite-Free Lithium Metal Anode. *ACS Appl. Mater. Interfaces* **2020,** *12* (28), 31542-31551.

[11] Xu, W.; Wang, J.; Ding, F.; Chen, X.; Nasybulin, E.; Zhang, Y.; Zhang, J.-G., Lithium metal anodes for rechargeable batteries. *Energy Environ. Sci.* **2014,** *7* (2), 513-537.

[12] Hong, Y.-S.; Zhao, C.-Z.; Xiao, Y.; Xu, R.; Xu, J.-J.; Huang, J.-Q.; Zhang, Q.; Yu, X.; Li, H., Safe Lithium-Metal Anodes for Li−O2 Batteries: From Fundamental Chemistry to Advanced Characterization and Effective Protection. *Batteries & Supercaps* **2019,** *2* (7), 638-658.

[13] Cheng, X.-B.; Zhao, C.-Z.; Yao, Y.-X.; Liu, H.; Zhang, Q., Recent Advances in Energy Chemistry between Solid-State Electrolyte and Safe Lithium-Metal Anodes. *Chem* **2019,** *5* (1), 74-96.

[14] Li, W.; Yao, H.; Yan, K.; Zheng, G.; Liang, Z.; Chiang, Y.-M.; Cui, Y., The synergetic effect of lithium polysulfide and lithium nitrate to prevent lithium dendrite growth. *Nat. Commun.* **2015,** *6* (1), 7436.

[15] Chen, Y.; Yue, M.; Liu, C.; Zhang, H.; Yu, Y.; Li, X.; Zhang, H., Long Cycle Life Lithium Metal Batteries Enabled with Upright Lithium Anode. **2019,**

29 (15), 1806752.

[16] Zheng, J.; Kim, M. S.; Tu, Z.; Choudhury, S.; Tang, T.; Archer, L. A., Regulating electrodeposition morphology of lithium: towards commercially relevant secondary Li metal batteries. *Chem. Soc. Rev.* **2020,** *49* (9), 2701-2750.

[17] Bao, C.; Wang, B.; Liu, P.; Wu, H.; Zhou, Y.; Wang, D.; Liu, H.; Dou, S., Solid Electrolyte Interphases on Sodium Metal Anodes. *Adv. Funct. Mater.* **2020,** *30* (52), 2004891.

[18] Xie, J.; Wang, J.; Lee, H. R.; Yan, K.; Li, Y.; Shi, F.; Huang, W.; Pei, A.; Chen, G.; Subbaraman, R.; Christensen, J.; Cui, Y., Engineering stable interfaces for three-dimensional lithium metal anodes. *Sci. Adv.* **2018,** *4* (7), eaat5168.

[19] Wang, H.; Lin, D.; Xie, J.; Liu, Y.; Chen, H.; Li, Y.; Xu, J.; Zhou, G.; Zhang, Z.; Pei, A.; Zhu, Y.; Liu, K.; Wang, K.; Cui, Y., An Interconnected Channel-Like Framework as Host for Lithium Metal Composite Anodes. *Adv. Energy Mater.* **2019,** *9* (7), 1802720.

[20] Sun, C.; Li, Y.; Jin, J.; Yang, J.; Wen, Z., ZnO nanoarray-modified nickel foam as a lithiophilic skeleton to regulate lithium deposition for lithium-metal batteries. *J. Mater. Chem. A* **2019,** *7* (13), 7752-7759.

[21] Ni, S.; Tan, S.; An, Q.; Mai, L., Three dimensional porous frameworks for lithium dendrite suppression. *Journal of Energy Chemistry* **2020,** *44*, 73-89.

[22] Zou, P.; Wang, Y.; Chiang, S.-W.; Wang, X.; Kang, F.; Yang, C., Directing lateral growth of lithium dendrites in micro-compartmented anode arrays for safe

lithium metal batteries. *Nat. Commun.* **2018,** *9* (1), 464.

[23] Lin, D.; Liu, Y.; Liang, Z.; Lee, H. W.; Sun, J.; Wang, H.; Yan, K.; Xie, J.; Cui, Y., Layered reduced graphene oxide with nanoscale interlayer gaps as a stable host for lithium metal anodes. *Nat Nanotechnol* **2016,** *11* (7), 626-32.

[24] Sun, Y.; Zheng, G.; Seh, Zhi W.; Liu, N.; Wang, S.; Sun, J.; Lee, Hye R.; Cui, Y., Graphite-Encapsulated Li-Metal Hybrid Anodes for High-Capacity Li Batteries. *Chem* **2016,** *1* (2), 287-297.

[25] Ji, X.; Liu, D.-Y.; Prendiville, D. G.; Zhang, Y.; Liu, X.; Stucky, G. D., Spatially heterogeneous carbon-fiber papers as surface dendrite-free current collectors for lithium deposition. *Nano Today* **2012,** *7* (1), 10-20.

[26] Zhang, A.; Fang, X.; Shen, C.; Liu, Y.; Zhou, C., A carbon nanofiber network for stable lithium metal anodes with high Coulombic efficiency and long cycle life. *Nano Res.* **2016,** *9* (11), 3428-3436.

[27] Yang, C.-P.; Yin, Y.-X.; Zhang, S.-F.; Li, N.-W.; Guo, Y.-G., Accommodating lithium into 3D current collectors with a submicron skeleton towards long-life lithium metal anodes. *Nat. Commun.* **2015,** *6* (1), 8058.

[28] Yun, Q.; He, Y.-B.; Lv, W.; Zhao, Y.; Li, B.; Kang, F.; Yang, Q.-H., Chemical Dealloying Derived 3D Porous Current Collector for Li Metal Anodes. *Adv. Mater.* **2016,** *28* (32), 6932-6939.

[29] Lu, L.-L.; Ge, J.; Yang, J.-N.; Chen, S.-M.; Yao, H.-B.; Zhou, F.; Yu, S.-H., Free-Standing Copper Nanowire Network Current Collector for Improving Lithium Anode Performance. *Nano Lett.* **2016,** *16* (7), 4431-4437.

[30] Song, R.; Wang, B.; Xie, Y.; Ruan, T.; Wang, F.; Yuan, Y.; Wang, D.; Dou, S., A 3D conductive scaffold with lithiophilic modification for stable lithium metal batteries. *J. Mater. Chem. A* **2018,** *6* (37), 17967-17976.

[31] Wang, C.; Wang, D.; Dai, C., High-Rate Capability and Enhanced Cyclability of Rechargeable Lithium Batteries Using Foam Lithium Anode. *J. Electrochem. Soc.* **2008,** *155* (5), A390.

[32] Xie, K.; Wei, W.; Yuan, K.; Lu, W.; Guo, M.; Li, Z.; Song, Q.; Liu, X.; Wang, J.-G.; Shen, C., Toward Dendrite-Free Lithium Deposition via Structural and Interfacial Synergistic Effects of 3D Graphene@Ni Scaffold. *ACS Appl. Mater. Interfaces* **2016,** *8* (39), 26091-26097.

[33] Chi, S.-S.; Liu, Y.; Song, W.-L.; Fan, L.-Z.; Zhang, Q., Prestoring Lithium into Stable 3D Nickel Foam Host as Dendrite-Free Lithium Metal Anode. *Adv. Funct. Mater.* **2017,** *27* (24), 1700348.

[34] Ye, H.; Xin, S.; Yin, Y.-X.; Li, J.-Y.; Guo, Y.-G.; Wan, L.-J., Stable Li Plating/Stripping Electrochemistry Realized by a Hybrid Li Reservoir in Spherical Carbon Granules with 3D Conducting Skeletons. *J. Am. Chem. Soc.* **2017,** *139* (16), 5916-5922.

[35] Pei, F.; Lin, L.; Ou, D.; Zheng, Z.; Mo, S.; Fang, X.; Zheng, N., Self-supporting sulfur cathodes enabled by two-dimensional carbon yolk-shell nanosheets for high-energy-density lithium-sulfur batteries. *Nat. Commun. 8* (1), 482.

[36] Lu, S.; Chen, Y.; Wu, X.; Wang, Z.; Li, Y., Three-dimensional

sulfur/graphene multifunctional hybrid sponges for lithium-sulfur batteries with large areal mass loading. *Sci. Rep.* **2014,** *4*, 4629.

[37] Qie, L.; Zu, C.; Manthiram, A., A High Energy Lithium-Sulfur Battery with Ultrahigh-Loading Lithium Polysulfide Cathode and its Failure Mechanism. *Adv. Energy Mater.* **2016,** *6* (7), 1502459.

[38] Zhou, G.; Paek, E.; Hwang, G. S.; Manthiram, A., High‐Performance Lithium‐Sulfur Batteries with a Self‐Supported, 3D Li2S‐Doped Graphene Aerogel Cathodes. *Adv. Energy Mater.* **2016,** *6* (2), 1501355.

[39] Frazier, W. E., Metal Additive Manufacturing: A Review. *J. Mater. Eng. Perform.* **2014,** *23* (6), 1917-1928.

[40] Jiang, Y.; Wang, B.; Liu, A.; Song, R.; Bao, C.; Ning, Y.; Wang, F.; Ruan, T.; Wang, D.; Zhou, Y., In situ growth of CuO submicro-sheets on optimized Cu foam to induce uniform Li deposition and stripping for stable Li metal batteries. *Electrochim. Acta* **2020,** *339*, 135941.

[41] Feng, Z.; Min, W.; Viswanathan, V. V.; Swart, B.; Shao, Y.; Gang, W.; Chi, Z., 3D Printing Technologies for Electrochemical Energy Storage. *Nano Energy* **2017,** *40*, S221128551730513X.

[42] Saleh, M. S.; Li, J.; Park, J.; Panat, R., 3D printed hierarchically-porous microlattice electrode materials for exceptionally high specific capacity and areal capacity lithium ion batteries. *Addit. Manuf.* **2018,** *23*, 70-78.

[43] Park, Y.-G.; Min, H.; Kim, H.; Zhexembekova, A.; Lee, C. Y.; Park, J.-U., Three-Dimensional, High-Resolution Printing of Carbon Nanotube/Liquid Metal

Composites with Mechanical and Electrical Reinforcement. *Nano Lett.* **2019,** *19* (8), 4866-4872.

[44] Peng, M.; Wen, Z.; Xie, L.; Cheng, J.; Jia, Z.; Shi, D.; Zeng, H.; Zhao, B.; Liang, Z.; Li, T.; Jiang, L., 3D Printing of Ultralight Biomimetic Hierarchical Graphene Materials with Exceptional Stiffness and Resilience. *Adv. Mater.* **2019,** *31* (35), 1902930.

[45] Wang, S.-H.; Yin, Y.-X.; Zuo, T.-T.; Dong, W.; Li, J.-Y.; Shi, J.-L.; Zhang, C.-H.; Li, N.-W.; Li, C.-J.; Guo, Y.-G., Stable Li Metal Anodes via Regulating Lithium Plating/Stripping in Vertically Aligned Microchannels. **2017,** *29* (40), 1703729.

[46] Zuo, T.-T.; Wu, X.-W.; Yang, C.-P.; Yin, Y.-X.; Ye, H.; Li, N.-W.; Guo, Y.-G., Graphitized Carbon Fibers as Multifunctional 3D Current Collectors for High Areal Capacity Li Anodes. **2017,** *29* (29), 1700389.

[47] Li, Q.; Quan, B.; Li, W.; Lu, J.; Zheng, J.; Yu, X.; Li, J.; Li, H., Electro-plating and stripping behavior on lithium metal electrode with ordered three-dimensional structure. *Nano Energy* **2018,** *45*, 463-470.

[48] Park, J.; Jeong, J.; Lee, Y.; Oh, M.; Ryou, M.-H.; Lee, Y. M., Micro-Patterned Lithium Metal Anodes with Suppressed Dendrite Formation for Post Lithium-Ion Batteries. **2016,** *3* (11), 1600140.

[49] Modeling of Industrial Electroplating Processes with Comsol Multiphysics in Order to Optimize Treatment of Complex Parts. *ECS Meeting Abstracts* **2019**.

[50] Yamaki, J.-i.; Tobishima, S.-i.; Hayashi, K.; Keiichi, S.; Nemoto, Y.;

Arakawa, M., A consideration of the morphology of electrochemically deposited lithium in an organic electrolyte. *J. Power Sources* **1998,** *74* (2), 219-227.

[51] Kushima, A.; So, K. P.; Su, C.; Bai, P.; Kuriyama, N.; Maebashi, T.; Fujiwara, Y.; Bazant, M. Z.; Li, J., Liquid cell transmission electron microscopy observation of lithium metal growth and dissolution: Root growth, dead lithium and lithium flotsams. *Nano Energy* **2017,** *32*, 271-279.

[52] Chen, C.; Jiang, J.; He, W.; Lei, W.; Hao, Q.; Zhang, X., 3D Printed High-Loading Lithium-Sulfur Battery Toward Wearable Energy Storage. *Adv. Funct. Mater.* **2020,** *30* (10), 1909469.

TOC

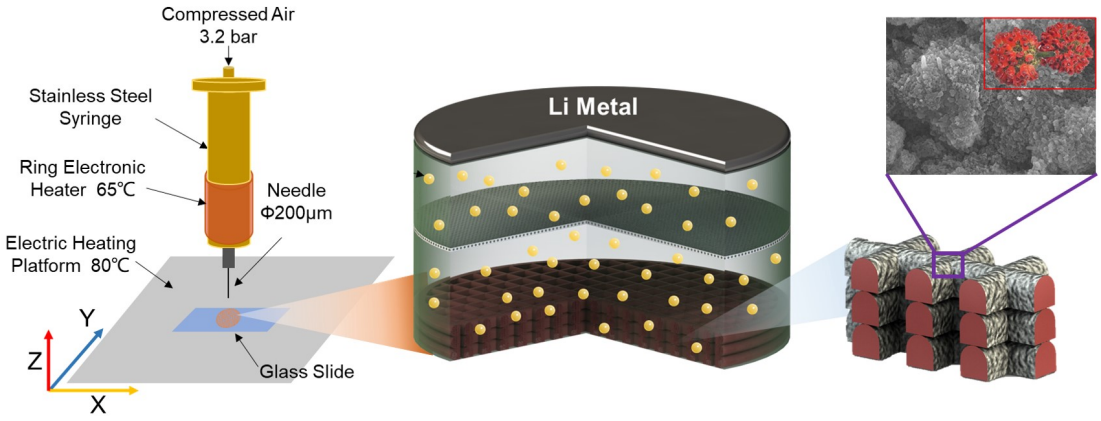

3D printed metal electrodes for lithium anodes demonstrate excellent deep peeling and plating capability, high rate capability and long cycle life.

ASSOCIATED CONTENT Supporting Information Available: Supporting information includes three video materials and specific experimental details.